



Contents lists available at ScienceDirect

## Computers &amp; Geosciences

journal homepage: [www.elsevier.com/locate/cageo](http://www.elsevier.com/locate/cageo)Method for rapid high-frequency seismogram calculation<sup>☆</sup>Tony Alfredo Stabile<sup>a,\*</sup>, Raffaella De Matteis<sup>b,1</sup>, Aldo Zollo<sup>a,2</sup><sup>a</sup> Dipartimento di Scienze Fisiche, Università di Napoli Federico II (RISSC-Lab), Via Diocleziano 328, 80125 Napoli, Italy<sup>b</sup> Dipartimento di Studi Geologici ed Ambientali, Università degli Studi del Sannio, Benevento, Italy

## ARTICLE INFO

## Article history:

Received 1 August 2007

Received in revised form

13 February 2008

Accepted 26 February 2008

## Keywords:

Synthetic seismogram

Ray theory

FORTRAN 77

Hierarchical generation

Physical constraint

## ABSTRACT

We present a method for rapid, high-frequency seismogram calculation that makes use of an algorithm to automatically generate an exhaustive set of seismic phases with an appreciable amplitude on the seismogram. The method uses a hierarchical order of ray and seismic-phase generation, taking into account some existing constraints for ray paths and some physical constraints. To compute synthetic seismograms, the COMRAD code (from the Italian: “COdice Multifase per il RAY-tracing Dinamico”) uses as core a dynamic ray-tracing code. To validate the code, we have computed in a layered medium synthetic seismograms using both COMRAD and a code that computes the complete wave field by the discrete wave number method. The seismograms are compared according to a time–frequency misfit criteria based on the continuous wavelet transform of the signals. Although the number of phases is considerably reduced by the selection criteria, the results show that the loss in amplitude on the whole seismogram is negligible. Moreover, the time for the computing of the synthetics using the COMRAD code (truncating the ray series at the 10th generation) is 3–4-fold less than that needed for the AXITRA code (up to a frequency of 25 Hz).

© 2008 Elsevier Ltd. All rights reserved.

## 1. Introduction

The calculation of synthetic seismograms has recently become a useful tool in seismological research, and a wide variety of techniques have been developed. Forward modelling, which means in this case the generation of synthetic seismograms, represents an important part of many seismological studies, such as seismic tomography or the kinematic inversion of source parameters (Pengcheng and Archuleta, 2004). The solution of an inverse problem requires the repeated solving of the forward problem, so that speed is the most stringent condition that the method must supply.

For horizontally stratified Earth models the complete wave field computation can be performed by using the theory of normal mode (Aki and Richards, 2002; Rosenbaum, 1960) or the discrete wave number method (Bouchon and Aki, 1977). Methods based on the direct numerical solution of the elastodynamic equation by finite difference (Madariaga, 1976; Virieux, 1986), finite elements (Marfurt, 1984), spectral elements (Festa and Vilotte, 2005; Komatitsch and Vilotte, 1998), or discontinuous Galerkin method (Kaser and Dumbser, 2006) can be applied to study the seismic wave field in a complex laterally varying structure.

As an alternative it is possible to obtain the solution to the wave equation by using approximate high-frequency methods (Cerveny, 2001). The solution of the elastodynamic equation is composed of elementary body waves that correspond to the various rays connecting the source to the receiver. Although the computation of ray synthetic seismograms is only approximate and the ray method can fail in certain situations, the high-frequency methods are preferable to direct numerical methods for many

<sup>☆</sup> Code available from server at <http://www.iamg.org/CGEditor/index.htm>.

\* Corresponding author. Tel.: +39 81 2420327; fax: +39 81 2420334.

E-mail addresses: [stabile@na.infn.it](mailto:stabile@na.infn.it) (T.A. Stabile),

[dematteis@unisannio.it](mailto:dematteis@unisannio.it) (R. De Matteis), [zollo@na.infn.it](mailto:zollo@na.infn.it) (A. Zollo).

<sup>1</sup> Tel.: +39 824 323658; fax: +39 81 2420334.

<sup>2</sup> Tel.: +39 81 2420315; fax: +39 81 2420334.

applications, both for the shorter computing times and for the full interpretability of the seismograms. The problems arise when we want to use a synthetic seismogram as similar to the real one as possible in the high-frequency approximation, such that the seismogram should be relatively complete, although it is not necessary that it contains every feature of the full elastic wave field. It is becoming necessary to select from all of the rays connecting the source to the receiver only those that produce an appreciable amplitude on the seismogram. The problem of generating a comprehensive set of rays was approached for the first time by Hron (1971, 1972) and Hron et al. (1986) for layered media, by grouping individual rays into families of kinematic equivalents. Afterwards, Clarke (1993a,b) developed a technique for computing synthetic seismograms based on a ray-generation algorithm that involved the symbolic manipulation of complete wave field expressions from the reflectivity theory, which were truncated to produce a finite ray series.

In this study, we propose a new technique for the rapid definition of an exhaustive set of rays that is based on the hierarchic generation of strings that describe the ray paths and the phase types. The string generation is subjected to physical constraints that are related to the propagation medium and the source–receiver geometry. The ray sets will represent the input of a kinematic or dynamic ray-tracing algorithm (i.e. Cerveny and Hron, 1980; Farra and Madariaga, 1987; Snieder and Spencer, 1993; Virieux, 1991). In particular, the technique developed has been implemented in the multiphase dynamic ray-tracing COMRAD code (from the Italian: “CODice Multifase per il RAY-tracing Dinamico”) that uses as its core the dynamic ray-tracing code provided by Farra and Madariaga (1987).

## 2. Method

Our goal is to develop an algorithm that rapidly generates an exhaustive number of seismic phases to calculate a high-frequency seismogram as complete as possible. In particular, the computing time is a critical parameter when the computation of synthetic seismograms has to be repeated many times in the inversion processes. The amplitudes, the ray paths and the travel times of the seismic phases are computed by the dynamic ray-tracing code provided by Farra and Madariaga (1987). In this section we describe our method and the discretization of the propagation model.

### 2.1. General concepts

It is possible to use an arbitrary medium as long as it is discretized by  $M$  ordered elements between a free surface and a halfspace. The sequential elements are separated by a surface. Each element can have an arbitrary shape and is characterized by the following properties:

- $Vp_i$ : compressive wave velocity (P-wave);
- $Vs_i$ : shear wave velocity (S-wave);
- $\tilde{n}_i$ : density;

- $Qp_i$ : P-wave quality factor (optional);
- $Qs_i$ : S-wave quality factor (optional);
- $T_i$ : top surface of the element;
- $B_i$ : bottom surface of the element ( $= T_{i+1}$ : top surface of the next element);
- $i = 1, \dots, M$ : index of the element.

where the elastic wave velocities, densities, and quality factors are functions of spatial coordinates.

Both the source and the receivers take the index  $i$  of the element in which they are included. Each ray goes from the source to the receiver and is divided into  $L$  curves if it passes through  $L$  elements. Each ray is described by a numerical string composed of  $L$  numbers, and each one is the index of the element crossed by the ray. For a ray there are also  $2^L$  phase numerical strings, because in each element crossed by the ray the wave can have two different polarizations (P-wave or S-wave). A numerical string for a phase is composed of  $L$  numbers and each one can be 1 (to indicate a P-wave) or 2 (to indicate an S-wave).

As an example, we can consider a medium where the elements are three horizontal, parallel layers, with a source inside the third layer, and a receiver inside the first layer. In this case, the ray path of the direct wave is described by the ray string 3–2–1 at which correspond  $2^3$  phase strings.

Although the algorithm can generate only body waves, it is possible to calculate headwaves' travel times using an artefact. We can consider a tiny element between two elements, with the same properties of the second one, and generate a ray string relative to a wave that propagates inside the tiny element. The travel time obtained for that wave is about equal to that for a headwave, but the amplitude is not correct.

### 2.2. Selection criteria

Once the length  $L$  of the numerical ray string is fixed, there are  $M^L$  ray strings of the same length if the medium is discretized by  $M$  elements. However, not all of the ray strings describe a real ray, because there are some existence constraints for a ray path:

- (a) The ray starts at the source;
- (b) the ray arrives at the receiver;
- (c) the ray path is bordered by the free surface and the half space;
- (d) if a ray points towards the top surface of the  $i$ th element, it can remain in the same element (with opposite direction) or go to the  $(i-1)$ th element (with the same direction);
- (e) if a ray points towards the bottom surface of the  $i$ th element, it can remain in the same element (with opposite direction) or go to the  $(i+1)$ th element (with the same direction);
- (f) if the receiver is on the free surface, the ray must come from below;
- (g) if the source is on the free surface, the starting direction of each ray cannot be up.

To generate only the ray strings that describe real ray paths, we use a hierarchic order of ray generation, where the root (first generation) is the index of the element that contains the source, and the number of generations is the length of the numerical strings of the rays. The hierarchic order of ray generation satisfies itself for the (a), (b), and (c) constraints. Indicating with  $S$  the source index and with  $R$  the receiver index, the generation that produce the ray string of minimum length, that is the direct ray, is given by the number  $Lmin = |S-R|+1$ . An example of hierarchic ray generation taken to the fourth generation for a source in the third element ( $S = 3$ ) and a receiver in the first element ( $R = 1$ ), where the medium is discretized by  $M = 5$  elements, is shown in Fig. 1. In this case we have, on the whole, four ray strings (3–2–1, 3–2–1–1, 3–3–2–1, and 3–2–2–1) up to the fourth generation that satisfy the (a), (b), and (c) constraints.

Using the additional (d), (e), (f), and (g) constraints, we discard some branches inside the numerical string tree. In particular, putting the receiver on the free surface the ray strings selected are shown in Fig. 2. Now we have only two ray strings (3–2–1 and 3–3–2–1) up to the fourth generation. If we put the receiver inside the first element instead of on the free surface, we will have the additional ray string 3–2–1–1 because there is no (f) constraint yet, and consequently the ray can arrive at the receiver also from above.

Since the number of phase strings becomes greater and greater if the number of generations increases, and consequently the computing time rises, it is possible to

introduce some constraints on the propagation in order to reduce the number of phases. For this reason, we created the following additional constraints on ray paths and phases:

- (I) Maximum number of generations that means the truncation of ray series;
- (II) maximum number of reflections in each element;
- (III) phase selection based on their expected amplitude values.

In agreement with the ray theory there are infinite rays that propagate from the source to the receiver, but there is also a loss of the initial ray energy whenever it has a reflection/transmission on a discontinuity, besides the energy lost for geometric and anelastic attenuation. After a certain number of generations, the ray strings represent those rays that have encountered so many discontinuities as to have a negligible energy. For this reason it is possible to truncate the ray series at a certain generation without significant loss in energy, this is the principle on which is founded the (I) constraint. In particular, the default maximum number of generation is fixed by the number  $Lmax = Lmin+2M$ , which guarantees a complete investigation of the propagation medium.

The (II) constraint assumes that a ray trapped inside an element has a loss in energy bigger than the energy lost by untrapped rays, especially for deeper elements. Using the (II) constraint, a ray string will be accepted only if it satisfies the condition:

$$(n - 1)i \leq RIFM \tag{1}$$

with  $n$  is the number of consecutive multiple reflections of the ray inside the  $i$ th element,  $i$  the element index, and  $RIFM$  a number that controls the multiple reflections (the default value is  $RIFM = 8$ ). Using the  $RIFM$  default value we can have maximum nine consecutive reflections in the first element (the shallowest), five consecutive reflections in the second, three in the third and the fourth, two from the fifth to the eighth, and only one for the others.

The (III) constraint is developed following this scheme:

- For each  $k$ th component of the phase string a weight  $w_k$ , from 0 to 1, is assigned;
- once the weight is assigned, the phase string will be accepted only if it satisfies the condition:

$$\prod_{k=1}^L w_k \geq PHS \tag{2}$$

where  $L$  is the length of the phase string and  $PHS$  is a number that represents a percentage of the weights product assigned to the direct P-wave (the default percentage is  $1 \times 10^{-4}\%$ ).

Here we describe how the weights  $w_k$  have been calculated. For each incident phase (P or S) on the boundary between two elements, we have to calculate each time the scattering coefficient relative to one of the eight phases that can be generated for reflection/transmission/conversion (PrP, PrS, PtP, PtS, SrP, SrS, StP, StS;

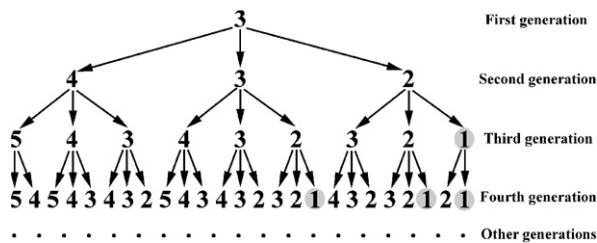


Fig. 1. Tree structure of ray strings stopped to fourth generation. Root, that is source position, is number three. Grey circles identify, for each generation, last component of strings that satisfy the (b) selection criterion. We have four ray strings up to fourth generation.

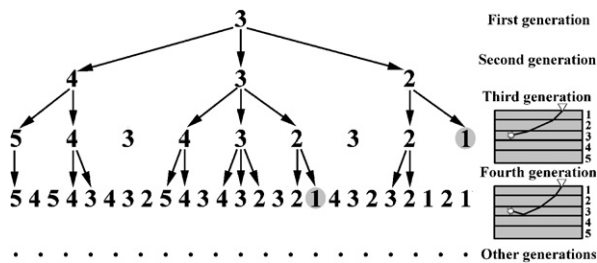


Fig. 2. Tree structure of ray strings stopped to fourth generation as in Fig. 1, but using all of (a)-(g) constraints. There are only two ray strings up to fourth generation because the receiver is on free surface. If the receiver is inside the first element, there will also be string 3–2–1–1. Ray paths relative to two selected ray strings in a layered velocity model are shown on right. White star is for source and white triangle is for receiver.

where  $r$  indicates the reflection and  $t$  the transmission). These coefficients are functions of the incidence angle and the physical parameters (P-wave velocity, S-wave velocity, and density) of the elements crossed by the wave. Their calculation requires both computing time and the values of the incidence angles, but the latter are known only after ray tracing. To overcome the problem, the weights  $w_k$  are defined for each type of interface and for each type of phase independent of the incidence angle. Indeed, to define the weights, we have calculated, for each one of the eight scattering coefficients, the integral on the whole interval of the incidence angle, dividing the result for the same interval. The values obtained for the four phases that an incident wave can generate (PrP, PrS, PtP, PtS for a P-wave; SrP, SrS, StP, StS for an S-wave) are normalized such that their sum is equal to one. This computation is carried out varying the interface parameters, that is the values of the P-wave velocities, S-wave velocities, and densities of the elements separated by discontinuity (Table 1). Precisely, S-wave velocities have been determined from P-wave velocities using different values of the  $V_p/V_s$  ratio, while densities have been calculated using the following empirical formula of Ludwig et al. (1970):

$$\rho = 0.7 + 2.23v - 0.598v^2 + 0.0704v^3 - 0.00283v^4 \quad (3)$$

with  $\rho$  the density in  $g/cm^3$  and  $v$  the P-wave velocity in km/s. The results show that for an incident P-wave the value of the integral, defined previously, depends essentially on the  $V_{p1}/V_{p2}$  ratio (indexes 1 and 2 indicate the medium that contains the incident wave and the medium that contains the transmitted wave, respectively). Likewise for an incident S-wave the integral depends on the  $V_{s1}/V_{s2}$  ratio. In fact, as shown in Figs. 3 and 4, the curves relative to the different cases reported in Table 1 have a similar shape for each type of phase (i.e. PtP, PrP, etc.).

To avoid the construction of an indexed table for each phase and for each value of  $V_{p1}/V_{p2}$  and  $V_{s1}/V_{s2}$  we have selected only five intervals of these ratios. The weight assigned to each phase will correspond to the maximum of the corresponding integral curve inside each region. This allows the realization of a smaller indexed table (Table 2) that contains the weights to assign to the components of the phase strings. Moreover, the weight assigned to a component of the phase string is equal to zero if in the  $i$ th element the component indicates an S-wave and  $V_{s_i} < 0.1$  m/s. From Eq. (2) this implies that the whole phase string is rejected.

**Table 1**

Different velocity models to study the effect of boundary between an half-space that contains incident wave (labelled by number 1) and an half-space that contains transmitted wave (labelled by number 2)

Velocity model	$V_{p1}$ (km/s)	$V_{p1}/V_{s1}$	$V_{p2}$ (km/s)	$V_{p2}/V_{s2}$
A	2.50	1.73	1.8–7.0	1.73
B	7.00	1.73	1.8–7.0	1.73
C	3.40	1.73	1.8–7.0	3.50
D	4.00	3.50	1.8–7.0	1.73
E	4.00	2.00	1.8–7.0	2.00

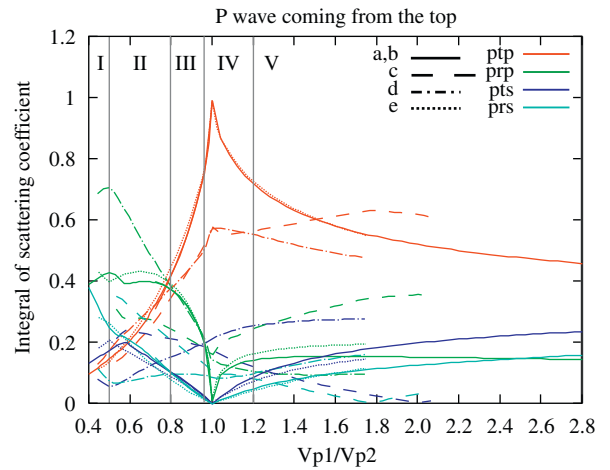


**Fig. 3.** Integral of scattering coefficients for an incident P-wave, as a function of  $V_{p1}/V_{p2}$  ratio between P-wave velocity in medium 1 (that contains incident wave) and P-wave velocity in medium 2 (that contains transmitted wave). Colour of curves refers to different type of phases, while style of curves is relative to different velocity models reported in Table 1. Five regions I, II, III, IV, and V, separated by vertical lines, are defined in Table 2.

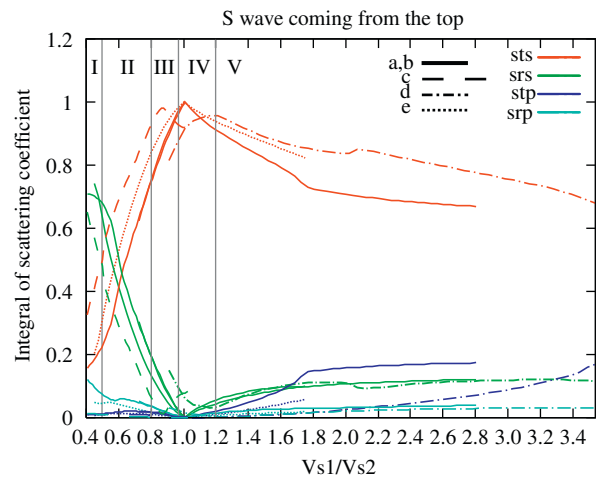


**Fig. 4.** As for Fig. 3 but referring to an incident S-wave as a function of  $V_{s1}/V_{s2}$  ratio between S-wave velocity in medium 1 and S-wave velocity in medium 2.

### 3. Structure of the COMRAD code

The Comrad.f code is the Fortran77 version of multi-phase code that, based on selection criteria, generates an exhaustive set of ray and phase strings allowing the computation of a seismogram as complete as possible. In order to compute synthetic seismograms, that is travel times, amplitudes, and ray paths relative to the selected phases, it uses as its core the dynamic ray-tracing code developed by Farra and Madariaga (1987), which needs a medium discretized by flat tilted layers. However, the COMRAD code can be easily implemented with other dynamic ray-tracing programs that can work on 3-D models with irregular discontinuities. The code is

**Table 2**

Weights assigned for each region, defined by  $z$  parameter, and for each type of phase

Type of phase	Region I $z < 0.5$	Region II $0.5 < z < 0.8$	Region III $0.8 < z < 0.95$	Region IV $0.95 < z < 1.2$	Region V $1.2 < z$
PrP	0.17	0.45	0.73	1.00	0.71
PrP	0.70	0.69	0.37	0.24	0.35
PrS	0.21	0.24	0.21	0.25	0.27
PrS	0.51	0.35	0.19	0.12	0.21
StS	0.50	0.92	0.98	1.00	0.96
SrS	0.90	0.66	0.19	0.10	0.16
SpP	0.01	0.02	0.02	0.02	0.17
SrP	0.17	0.07	0.03	0.03	0.05

$z$  parameter is equal to  $V_{p1}/V_{p2}$  ratio for an incident P-wave or equal to  $V_{s1}/V_{s2}$  ratio for an incident S-wave.

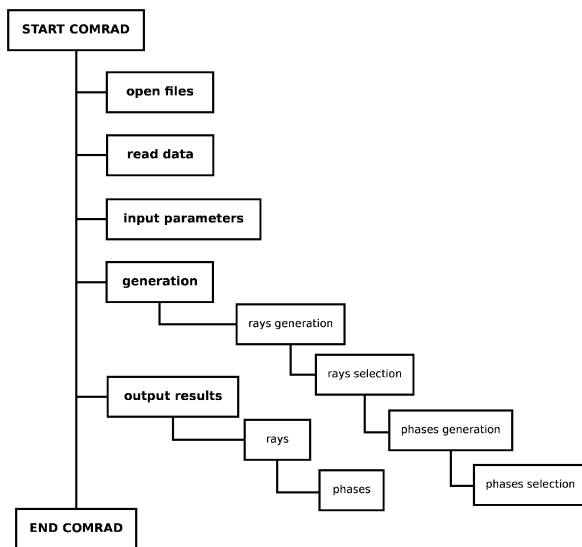


**Fig. 5.** Block scheme of the Comrad.f computer code.

accompanied by the bash script `multiphase.sh`, which optimizes the whole calculation process and runs both the COMRAD and core programs.

The structure of the code is shown in Fig. 5, where we outline its most important features. The code requires the following input data:

- a file (`creation.inp`) that contains the medium information;
- a file (`xxxx.dis`, where `xxxx` represents a four-character word) that contains the source–receiver geometry;
- the maximum number of generations ( $Lmax$ ), which truncates the ray series. The user can choose to use the default value ( $Lmax = Lmin + 2m$ );
- the multiple reflections parameter ( $RIFM$ ), which allows the ray to have a finite number of reflections in each element. The user can choose to use the default value ( $RIFM = 8$ );
- the phase selection parameter ( $PHS$ ), which discards phases with negligible amplitudes. The user can choose to use the default value (calculated on the

approximated amplitude value of the direct P-wave and fixed at  $1 \times 10^{-4}$  of this value);

- the initial polarization of the phases (P or S). Using the hierarchical generation method with the constraints described previously, the code generates the ray and phase strings and creates the following output data:
  - a file (`kernel.inp`) that contains the input parameters for the core;
  - two files (`xxx1.dis` and `xxx2.dis`, where `xxx` represents a three character word) inside which the Comrad.f code will write all of the ray and phase strings to be used by the core program for the computation of the synthetics. The first file describes rays where their starting direction is up, and the second, where it is down. These two files are very important also to search the type of phase identified on the output seismograms, since they contains the list of the ray and phase strings.

The existence of the two `xxx1.dis` and `xxx2.dis` files assures the calculations of both the  $P/P\backslash$  (where  $S/\backslash$  or  $P/\backslash$  indicates an upcoming S- or P-wave and  $S\backslash$  or  $P\backslash$  a downgoing S- or P-wave, respectively) and  $P\backslash P/$  phases (and similar), although they are described by the same ray and phase strings if the source and the receiver are both in the same element (i.e. the ray string is 1–1 both for  $P/P\backslash$  and  $P\backslash P/$  phases if the source and the receiver are in the first element of the medium). Moreover, if the source is on the free surface, the `xxx1.dis` does not exist because of the (g) constraint.

In order to select the appropriate weight for each type of phase we have transformed Table 2 in a 3D-matrix of indexes  $Z$ ,  $RT$ , and  $POL$ . The  $RT$  index indicates if there is a reflection or a transmission; it is equal to 1 for a transmission and 2 for a reflection. The  $POL$  index indicates the polarization of the phase before and after a reflection/transmission; it is equal to 1 for PP, 2 for PS, 3 for SP, and 4 for SS.  $Z$  indicates the number of the region (see Figs. 3 and 4) containing the  $V_{p1}/V_{p2}$  ratio (for an incident P-wave) or  $V_{s1}/V_{s2}$  ratio (for an incident S-wave) values. To avoid the introduction in the `comrad.f` program a great number of control instructions to verify the index values, we have searched two relations (Eqs. (4) and (5)) that directly determine the values of the  $RT$  and  $POL$  indexes. The value of the  $RT$  index is obtained from Eq. (4):

$$RT = |ud1 - ud2| + 1 \quad (4)$$

with  $ud1$  and  $ud2$  are the directions (1 for up and 2 for down) of the  $i$ th component and the  $i+1$ th component of the ray string, respectively. The value of the  $POL$  index is obtained instead from Eq.(5):

$$POL = 2a + b - 2 \quad (5)$$

where  $a$  and  $b$  are the polarizations (1 for a P-wave and 2 for an S-wave) of the  $i$ th component and the  $i+1$ th component of the phase string, respectively.

After the COMRAD and core programs have finished, the output consists of files containing the Green function and a list of ray paths, travel times and amplitudes for all the phases. If more than one receiver is considered it is

possible to produce a synthetic section for each component ( $X$ ,  $Y$ , and  $Z$ ).

#### 4. Validation of the method

The higher the number of generations we consider, the higher the number of phases the core must calculate. To make the best choice on the number of generations, we have to compare the calculation time with the complexity we need for the synthetics. We compute synthetic seismograms for two receivers ( $R_1$  and  $R_2$ ), respectively, at 1 and 30 km distance from the epicentre of an explosive source. The source function is a triangle with a duration of 0.1 s, but it is possible to choose other source functions (i.e. Sinusoidal, Gaussian, Ricker, etc.) and change the duration and the frequency. We use a crustal velocity model (Bernard and Zollo, 1989), where the elements are considered in this case as horizontal parallel layers. The model is described in Table 3, while the results of the simulations are given in Table 4. Only the geometrical spreading is considered in the computation of synthetics and no headwaves are considered since we can compute only their travel times and not the amplitudes.

The source depth is 4 km, and both of the receivers are at 1 m in depth. For this source–receiver geometry, the source is in the second layer, the receivers are in the first layer and the first real phases start at the second generation. In Table 4, for each generation, the time needed by both the COMRAD and core programs for the calculations can be seen, along with the total number of phases and the RMS calculated for both of the receivers and for both of the  $X$  and  $Z$  components of the seismogram. The RMS is a measure of the similarity

between two signals and in Table 4 it is calculated between the synthetic seismogram obtained at each generation ( $S(t)$ ) and that obtained for the previous generation ( $S_{REF}(t)$ ). The RMS is defined as follows:

$$RMS = \sqrt{\frac{\sum_t |S(t) - S_{REF}(t)|^2}{\sum_t |S_{REF}(t)|^2}} \quad (6)$$

where  $t$  is the time. The amplitudes of the seismograms are normalized with respect to their maximum amplitudes. The calculations are carried out using a PC with an AMD-3 GHz processor and 2 Mb SD-RAM memory.

We show the results up to the 12th generation since the RMS becomes negligible at the expense of an excessive computing time. From Table 4, it is clear that the RMS is lower and lower as a function of the number of generations. Moreover, starting from the RMS calculated between the 9th and 10th generations, the RMS decrease rate at 30 km distance becomes stable for both the  $X$  and  $Z$  components. This means that if we truncate the ray series at the 10th generation we obtain little values both for the RMS and the computing time.

If we take into account also the propagation constraints it is possible to reduce further the number of phases created at each generation. The selection on the phase strings is controlled by the RIFM and the PHS parameters discussed in the previous paragraph. In order to evaluate the changes on the seismogram due to the application of these constraints, we calculate the RMS, the computing time, and the number of phases for different values of RIFM and PHS parameters. In particular we used  $RIFM = \infty$ , when the constraint is not used, and the default value  $RIFM = 8$ . The test is performed on the seismogram obtained at the 10th generation for both receivers  $R_1$  and  $R_2$  of the previous model. The RMS is computed using as reference signal both the same seismogram but complete with all phases and the seismogram computed at the 12th generation complete with all phases. As we can see in Table 5 the use of the RIFM parameter can reduce the number of phases (and then the computing time) from 2% to 20%, but this reduction depends on the choice of the PHS value (it is bigger for lower PHS values). On the other hand, PHS is a crucial parameter able to reduce considerably the number

**Table 3**  
Crustal velocity model used for simulations

Interfaces	Depth (km)	Vp (km/s)	Vs (km/s)	$\rho$ (g/cm <sup>3</sup> )
1	0	2.30	1.33	2.2
2	3	5.30	3.06	2.3
3	7	6.00	3.46	2.4
4	10	6.28	3.63	2.6
5	20	6.54	3.78	2.8

**Table 4**  
Computing time of COMRAD and core codes, number of phases, and RMS computed at each generation for both receivers  $R_1$  and  $R_2$ , at 1 and 30 km distance from the source, respectively

N. GEN.	Comrad time (s)	Core time (s)	N. phases	RMS $R_1$ -CompX	RMS $R_1$ -CompZ	RMS $R_2$ -CompX	RMS $R_2$ -CompZ
2	0 m 00.05	0 m 00.06	2	–	–	–	–
3	0 m 00.05	0 m 00.15	10	1.037	0.992	4.628	4.789
4	0 m 00.05	0 m 00.29	34	0.108	0.104	0.980	0.932
5	0 m 00.05	0 m 01.13	114	0.107	0.103	0.262	0.340
6	0 m 00.05	0 m 04.42	370	0.027	0.144	0.440	0.494
7	0 m 00.05	0 m 16.84	1266	0.026	0.028	0.398	0.399
8	0 m 00.05	1 m 07.45	4210	0.008	0.010	0.186	0.252
9	0 m 00.11	4 m 18.82	14,706	0.008	0.010	0.131	0.220
10	0 m 00.27	16 m 18.15	49,522	0.002	0.004	0.087	0.109
11	0 m 01.18	1 h 00 m 23.47	174,450	0.002	0.004	0.077	0.092
12	0 m 03.39	3 h 40 m 56.38	590,194	0.001	0.002	0.037	0.058

**Table 5**

Horizontal (CompX) and vertical (CompZ) components of seismograms are considered.

Computing time of COMRAD (+core) code, number of phases, and RMS computed at each generation for both receivers  $R_1$  and  $R_2$ , at 1 and 30 km distance from the source, respectively

PHS (%)	RIFM	Comrad time (s)	N. phases	RMS-10th $R_1$ -CompZ	RMS-10th $R_2$ -CompZ	RMS-12th $R_1$ -CompZ	RMS-12th $R_2$ -CompZ
0	$\infty$	16 m 18.42	49,522	0.000	0.000	0.005	0.109
$1.4 \times 10^{-4}$	$\infty$	8 m 52.96	29,300	0.000	0.035	0.005	0.116
$1.4 \times 10^{-4}$	8	8 m 18.91	24,218	0.000	0.035	0.005	0.116
$1.4 \times 10^{-2}$	$\infty$	1 m 25.20	4648	0.000	0.298	0.005	0.319
$1.4 \times 10^{-2}$	8	1 m 18.31	4195	0.000	0.298	0.005	0.319
1.4	$\infty$	0 m 01.99	137	0.015	0.694	0.017	0.703
1.4	8	0 m 01.77	134	0.015	0.694	0.017	0.703

Vertical component (CompZ) of seismograms is considered. RMS-10th is the RMS relative to seismogram computed at 10th generation without constraints. RMS-12th is the RMS relative to seismogram computed at 12th generation without constraints.

of phases without losing the phases with bigger amplitude. If we choose for PHS a value equal to 1.4% of the relative direct P-wave value, the computing time is drastically reduced (from 16 m 18.15 s to 1.77 s), whereas the RMS becomes significant for the more distant receiver ( $R_2$ ). The best values for RIFM and PHS parameter can be chosen on the basis of the required precision.

To better understand if our choice is appropriate, we can calculate the complete wave field for the case under study by the AXITRA program, which uses the discrete wave number method developed by Bouchon (Bouchon, 1981; Cotton and Coutant, 1997). Afterwards, we can compare the AXITRA results with those obtained using the COMRAD program stopped at the 10th generation, where the amplitudes of the synthetics are expressed in velocity and are normalized with respect to their maximum amplitude. The AXITRA computation time (up to the frequency of 25 Hz) is 53 min and 41.6 s, 3–4-fold longer than the COMRAD+core computation time obtained at the 10th generation (see Table 5). For a quantitative comparison between the synthetics, we use the misfit criteria in time and frequency that was developed by Kristekova et al. (2006). In fact, the standard RMS matches the single-valued envelope misfit only in the case of a pure amplitude modification of the signal, while in all other cases RMS considerably overestimates the misfits and does not recognize what causes the difference (Kristekova et al., 2006). The time frequency envelope misfit (TFEM) is calculated according to the following equation:

$$TFEM(t, f) = \frac{\Delta E(t, f)}{\max_{t, f} (|W_{REF}(t, f)|)} \quad (7)$$

while the time frequency phase misfit is calculated according to Eq. (3):

$$TFPM(t, f) = \frac{\Delta P(t, f)}{\max_{t, f} (|W_{REF}(t, f)|)} \quad (8)$$

where  $t$  is the time,  $f$  is the frequency,  $\Delta E(t, f)$  is the local time–frequency envelope difference,  $\Delta P(t, f)$  is the local time–frequency phase difference, and  $W_{REF}(t, f)$  is the time–frequency representation of the reference signal  $S_{REF}(t)$  based on the continuous wavelet transform. In this case the difference is computed between the COMRAD and AXITRA seismograms.

In Figs. 6 and 7, the TFEM and the TFPM misfits for the vertical component of the seismograms computed at the receivers at 1 and 30 km distance from the source are shown. Red colour in the TFEM and the TFPM images indicates a greater amplitude and a positive phase shift in the COMRAD seismogram with respect to AXITRA seismogram. Blue colour represent the opposite case. For the receiver at 1 km distance the TFEM and the TFPM values suggest a good agreement between the synthetics computed using the two methods. In fact the maximum TFEM value, observed at 1.5 s, is about 4%, while the maximum TFPM value is about 0.6%. This agreement slowly decreases with the source–receiver distance as shown in Fig. 7 for the receiver at 30 km distance from the source.

In Fig. 7 we can see that there is a maximum envelope misfit, of about 20%, in correspondence of 7.5 and 11 s. These misfits are due to differences in amplitude between the two seismograms, as evidenced in the plots of the synthetics in Fig. 7. Over 16 s COMRAD seismogram amplitudes are generally underestimated probably for the absence of the surface waves calculated by AXITRA and not by COMRAD code. Moreover, from the TFPM plot in Fig. 7, the phase misfit is less than 7%. In general, the differences in amplitude and phase between the synthetic seismograms computed by the two codes decrease at higher frequencies as expected by theory. The misfits are shown only for frequencies greater than 3 Hz because the COMRAD code is valid only in the high-frequency approximation.

## 5. Conclusions and discussions

We have developed a method for rapid high-frequency seismogram computation based on a hierarchical order of ray and phase strings generation subjected to physical constraints. The method is used in a code (Comrad.f) to compute an exhaustive set of phases able to produce a complete body waves seismogram. It uses as core the dynamic ray-tracing code developed by Farra and Madariaga (1987).

We have numerically tested the method in two steps using a PC with an AMD-3 GHz processor and 2 Mb SD-RAM memory. First we evaluated, generation by

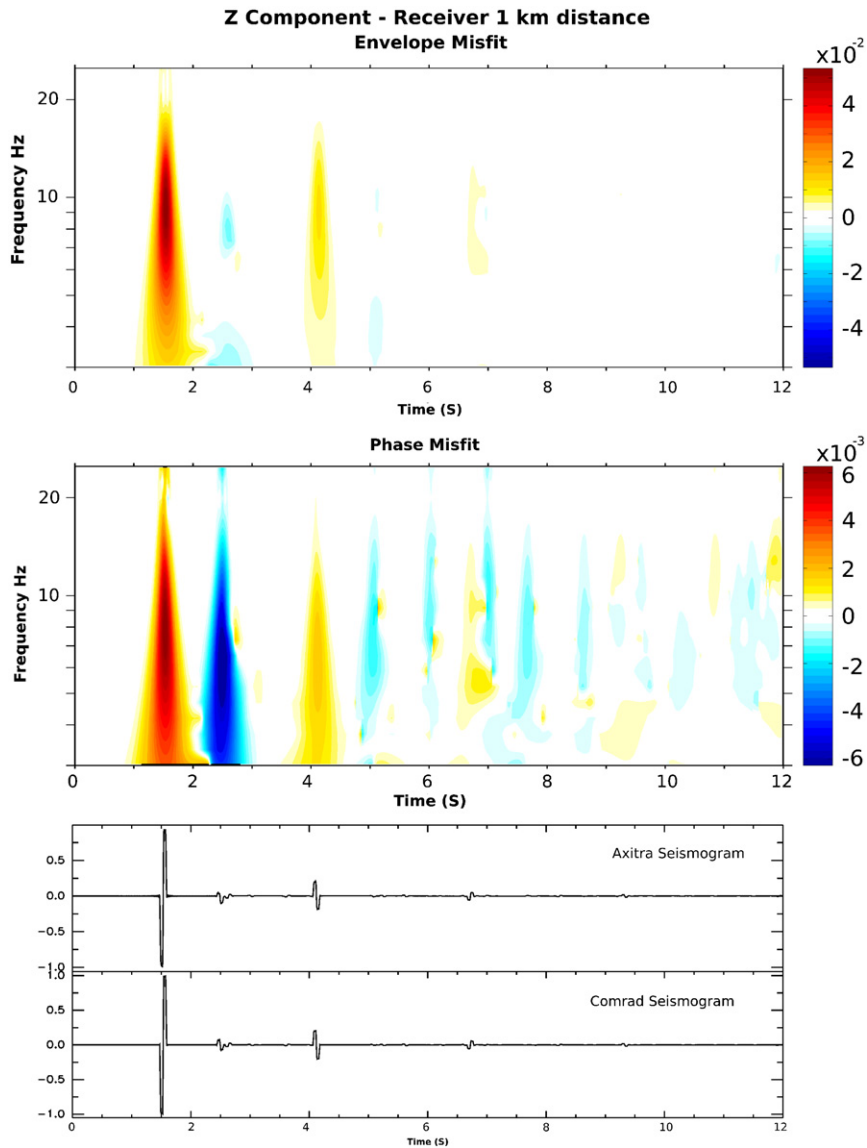


**Fig. 6.** (Top) Time frequency envelope misfit  $TFEM(t,f)$  and (Middle) time frequency phase misfit  $TFPM(t,f)$  plots for vertical components of seismograms computed for a receiver at 1 km distance from the source. (Bottom) Two synthetic seismograms computed by the AXITRA and COMRAD codes, respectively. Amplitudes are normalized with respect to maximum amplitude of each seismogram.

generation, both the computing time and the *RMS* between the COMRAD synthetics obtained in each generation and those obtained in the previous generation. This allowed us to choose the number of generation at which we can truncate the ray series, that is the 10th generation.

After fixing the number of generations, we compared the COMRAD-derived synthetic seismograms with AXITRA-derived synthetic seismograms, the latter being a program that calculates the complete wave field. The numerical tests were carried out by the quantitative misfit criteria developed by Kristekova et al. (2006).

The seismograms computed by the COMRAD and AXITRA programs are in good agreement at least up to 30 km source–receiver distance. For a receiver 30 km away

from the source, where we have greater misfits, the maximum time frequency envelope misfit is about 20% only corresponding to 7.5 and 11 s on seismograms, due to the differences in amplitudes.

Finally, we have compared the computation times for both of the programs, and we can be sure that the COMRAD code (with 10 generations without constraints) is 3–4-fold faster than the AXITRA code (up to a frequency of 25 Hz). If we want to compute the synthetics at higher frequencies, the AXITRA code needs more time, while the computation time of the COMRAD code remains the same or decreases if we take into account the additional constraints on the phases. These constraints are based on the maximum number of reflections in each element of the model and on the expected amplitude

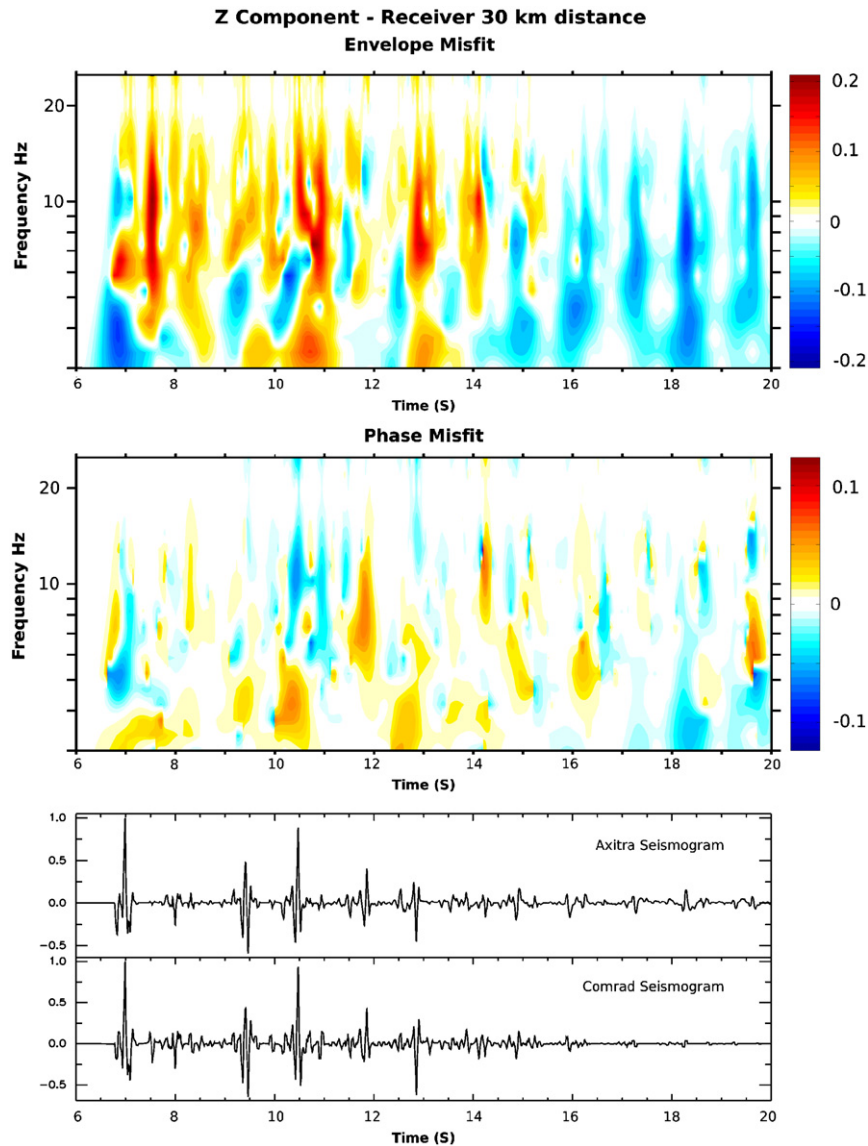


Fig. 7. As in Fig. 6 but referring to a receiver at 30 km distance from source.

value for each phase. We have evaluated the effects of these constraints on the seismogram computed at the 10th generation in terms of number of phases, computing time, and accuracy of the signal. The results confirm that the constraints are effective, reducing the number of phases to be computed without losing the phases with appreciable amplitude on the seismogram.

### Acknowledgements

The authors would like to thank Veronique Farra for providing us with her dynamic ray-tracing code, used as core of the COMRAD program. We are also grateful to Prof. Ray Durrheim for helpful suggestions and constructive comments on the manuscript.

### Appendix A. Supplementary material

Supplementary data associated with this article can be found in the online version at [doi:10.1016/j.cageo.2008.02.030](https://doi.org/10.1016/j.cageo.2008.02.030).

### References

- Aki, K., Richards, P.G., 2002. *Quantitative Seismology*, second ed. University Science Books, Sausalito, California, 720pp.
- Bernard, P., Zollo, A., 1989. The Irpinia (Italy) 1980 earthquake: detailed analysis of a complex normal faulting. *Journal of Geophysical Research* 94 (B2), 1631–1647.
- Bouchon, M., 1981. A simple method to calculate Green's functions for elastic layered media. *Bulletin of Seismological Society of America* 71 (4), 959–971.

- Bouchon, M., Aki, K., 1977. Discrete wave-number representation of seismic-source wave fields. *Bulletin of Seismological Society of America* 67 (2), 259–277.
- Cerveny, V., 2001. *Seismic Ray Theory*. Cambridge University Press, Cambridge, New York, 722pp.
- Cerveny, V., Hron, F., 1980. The ray series method and dynamic ray-tracing system for three-dimensional inhomogeneous media. *Bulletin of Seismological Society of America* 70, 47–77.
- Clarke, T.J., 1993a. The complete ordered ray expansion—I. Calculation of synthetic seismograms. *Geophysical Journal International* 115, 421–434.
- Clarke, T.J., 1993b. The complete ordered ray expansion—II. Multiphase body wave tomography. *Geophysical Journal International* 115, 435–444.
- Cotton, F., Coutant, O., 1997. Dynamic stress variations due to shear faults in a plane-layered medium. *Geophysical Journal International* 128 (3), 676–688.
- Farra, V., Madariaga, R., 1987. Seismic waveform modeling in heterogeneous media by ray perturbation theory. *Journal of Geophysical Research* 92 (B3), 2697–2712.
- Festa, G., Vilotte, J.P., 2005. The Newmark scheme as a velocity–stress time-staggering: an efficient perfectly matched layers implementation for spectral element simulations of elastodynamics. *Geophysical Journal International* 161 (3), 789–812.
- Hron, F., 1971. Criteria for selection of phases in synthetic seismograms for layered media. *Bulletin of Seismological Society of America* 61 (3), 765–779.
- Hron, F., 1972. Numerical methods of ray generation in multilayered media. In: Bolt, B.A. (Ed.), *Methods in Computational Physics*, vol. 12. Academic Press, New York, pp. 1–34.
- Hron, F., May, B.T., Covey, J.D., Daley, P.F., 1986. Synthetic seismic section for acoustic, elastic, anisotropic inhomogeneous layered media. *Geophysics* 51, 710–735.
- Kaser, M., Dumbser, M., 2006. An arbitrary high order discontinuous Galerkin method for elastic waves on unstructured meshes I: the two-dimensional isotropic case with external source terms. *Geophysical Journal International* 166 (2), 855–877.
- Komatitsch, D., Vilotte, J.P., 1998. The spectral element method: an efficient tool to simulate the seismic response of 2D and 3D geological structures. *Bulletin of Seismological Society of America* 88 (2), 368–392.
- Kristekova, M., Kristek, J., Moczo, P., Day, S.M., 2006. Misfit criteria for quantitative comparison of seismograms. *Bulletin of Seismological Society of America* 96 (5), 1836–1850.
- Ludwig, W.J.J., Nafe, E., Drake, C.L., 1970. *Seismic refraction*. In: Maxwell, A.E. (Ed.), *The Sea*. Wiley InterScience, Hoboken, New Jersey, pp. 53–84.
- Madariaga, R., 1976. Dynamics of an expanding circular fault. *Bulletin of Seismological Society of America* 66, 639–666.
- Marfurt, K.J., 1984. Accuracy of finite-difference and finite-element modeling of the scalar and elastic wave equations. *Geophysics* 49, 549–553.
- Pengcheng, L., Archuleta, R.J., 2004. A new nonlinear finite fault inversion with three-dimensional Green's functions: application to the 1989 Loma Prieta, California, earthquake. *Journal of Geophysical Research* 109 (B02318), 1–15.
- Rosenbaum, J.H., 1960. The long-time response of a layered elastic medium to explosive sound. *Journal of Geophysical Research* 65, 1577–1613.
- Snieder, R., Spencer, C., 1993. A unified approach to ray bending, ray perturbation, paraxial ray theories. *Geophysical Journal International* 115, 456–470.
- Virieux, J., 1986. P-SV wave propagation in heterogeneous media: velocity–stress finite-difference method. *Geophysics* 51, 889–901.
- Virieux, J., 1991. Fast and accurate ray tracing by Hamiltonian perturbation. *Journal of Geophysical Research* 96, 579–594.